ACS APPLIED MATERIALS & INTERFACES

Research Article

www.acsami.org

Highly Efficient, Solution Processed Electrofluorescent Small Molecule White Organic Light-Emitting Diodes with a Hybrid Electron Injection Layer

Zhixiong Jiang,[†] Zhiming Zhong,[†] Shanfeng Xue,[†] Yan Zhou,[‡] Yanhong Meng,[†] Zhanhao Hu,[†] Na Ai,[†] Jianbin Wang,[†] Lei Wang,[†] Junbiao Peng,[†] Yuguang Ma,[†] Jian Pei,[‡] Jian Wang,*[,†] and Yong Cao[†]

[†]Institute of Polymer Optoelectronic Materials and Devices, State Key Laboratory of Luminescent Materials and Devices, South China University of Technology, Guangzhou 510640, P. R. China

[‡]Key Laboratory of Bioorganic Chemistry and Molecular Engineering of Ministry of Education, College of Chemistry, Peking University, Beijing 100871, P. R. China

ABSTRACT: Highly efficient, solution-processed, and all fluorescent white organic light-emitting diodes (WOLEDs) based on fluorescent small molecules have been achieved by incorporating a low-conductivity hole injection layer and an inorganic−organic hybrid electron injection layer. The light-emission layer is created by doping a fluorescent π-conjugated blue dendrimer host (the zeroth generation dendrimer, G0) with a yellow-emitting fluorescent dopant oligo(paraphenylenevinylene) derivative CN-DPASDB with a doping ratio of 100:0.15 (G0:CN-DPASDB) by weight. To suppress excessive holes, the high-conductivity hole injection layer (PEDOT:PSS AI 4083) is replaced by the low-conductivity PEDOT:PSS CH 8000. To facilitate the electron injection, a hybrid electron injection layer is introduced by doping a methanol/water-soluble conjugated polymer poly[(9,9-bis(30-(*N*,*N*-dimethylamino)propyl)-2,7-fluorene)-alt-2,7-(9,9-dioctylfluorene)] ($PFNR_2$) with solution-processed cesium fluoride (CsF). The device achieves a maximum luminous efficiency of 17.0 cd A^{-1} and a peak power efficiency of 15.6 lm W^{-1} at (0.32, 0.37) with a color rendering index of 64.

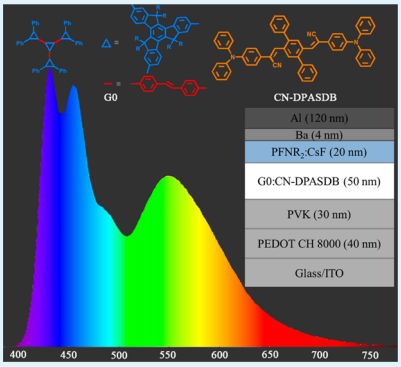

KEYWORDS: *white organic light-emitting diodes, electrofluorescent, solution process, cesium fluoride, inorganic−organic hybrid*

INTRODUCTION

Since their discovery, organic light-emitting diodes (OLEDs) have attracted enormous attention due to their potential applications in full-color flat-panel displays, backlights for liquid-crystal displays (LCD), and solid-state lighting sources.[1−5] Recently, white OLEDs (WOLEDs) for applications in solid-state lighting have become the focus of OLED development. In the literature, the power efficiency (PE) of the vacuum-deposited WOLEDs has reached 60 lm W^{-1},[6] while the PE of the solution-processed WOLEDs has approached 40 lm W^{-1},[7] for the devices without any substrate surface modifications. Currently, all state-of-the-art WOLEDs utilize phosphorescent emitters, which could reach 100% internal quantum efficiency.[8] Though the internal quantum efficiency of fluorescent emitters is capped at 25% due to the spin-conservation law, fluorescent emitters offer color stability, deep blue color coordinates, and less efficient roll-off at high current density compared with phosphorescent emitters.[9,10]

For small-molecule fluorescent emitters, Ma et al.[11] reported an all-fluorescent WOLED with a maximum luminous efficiency (LE) of 20.8 cd A^{-1} and a PE of 15.9 lm W^{-1} with color coordinates at (0.41, 0.41) by thermally evaporating red, green, and blue small molecules sequentially. For a conjugated polymer fluorescent emitter, by blending 9,9-bis(4-(2-ethylhexyloxy)phenyl)fluorene (PPF) based blue polymer (PPFSO), green polymer (PPF-SO-BT), and red polymer (PPF-SO-DHTBT) at an optimized ratio, Yang et al.[12] achieved a solution-processed white polymer light-emitting diode with a maximum LE of 9.8 cd A^{-1} and a PE of 8.9 lm W^{-1} at (0.35, 0.37). By doping a blue conjugated polymer polyfluorene (PF) with an orange light-emission small molecule dopant (rubrene), Yang et al.[13] demonstrated a highly efficient WOLED with a maximum LE of 17.9 cd A^{-1} and a PE of 16.3 lm W^{-1} at (0.33, 0.43). Combining the high efficiency of the small molecules and the solution-processability of the conjugated polymer, solution-processed small molecules have become an important research area in the field of OLEDs. Ma et al.[14] reported solution-processed fluorescent small-molecule WOLEDs with a maximum LE of 9.2 cd A^{-1} and a PE of 6.1 lm W^{-1} at (0.35,0.36) by mixing OCNzC (red), OCBzC (green), and OCPC (blue) as the light-emission layer.

In our contribution, we create a highly efficient fluorescent WOLED by doping a fluorescent π-conjugated blue dendrimer host G0 with a yellow-emitting fluorescent dopant oligo-(paraphenylenevinylene) derivative CN-DPASDB (Scheme 1). To balance the injected electrons and holes, in addition to

Received: February 27, 2014
Accepted: May 19, 2014
Published: May 19, 2014

   dx.doi.org/10.1021/am501207g | *ACS Appl. Mater. Interfaces* 2014, 6, 8345−8352

Scheme 1. Chemical Structures of G0, CN-DPASDB, and $PFNR_2$

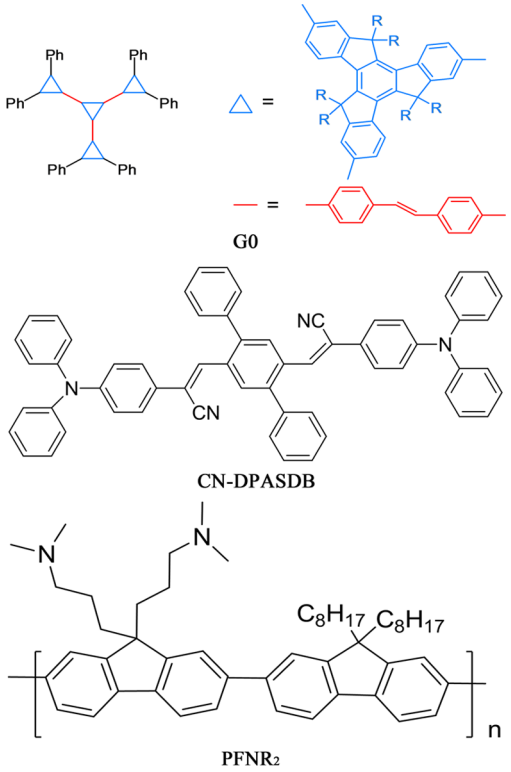

using a low conductive PEDOT:PSS (CH 8000) as the hole injection layer (HIL), we introduce a novel hybrid solution-processed electron injection layer (EIL): inorganic material cesium fluoride (CsF)-doped organic material poly[(9,9-bis(30-(*N*,*N*-dimethylamino)propyl)-2,7-fluorene)-alt-2,7-(9,9-dioctyl-fluorene)] ($PFNR_2$). The combination of low-conductivity HIL and hybrid EIL provides many balanced charge carriers in the emission layer. With balanced electrons and holes, the solution-processed fluorescent WOLED exhibits a highest forward-viewing PE of 15.6 lm W^{-1}, a peak LE of 17.0 cd A^{-1}, and an external quantum efficiency (EQE) of 6.45% at the CIE coordinates of (0.32, 0.37). The color-rendering index (CRI) reaches 64 at 13 mA cm^{-2}. To the best of our knowledge, the device efficiency is the highest ever reported for WOLEDs based on solution-processed fluorescent small molecules, which is also on par with the efficiency achieved by thermally evaporated fluorescent small molecules.

EXPERIMENTAL SECTION

Materials. The small molecules G0[15] and CN-DPASDB[16] used as emissive materials and the $PFNR_2$[17] used as the electron-injection material were synthesized in our laboratories. PVK and CsF were purchased from Aldrich. The PEDOT:PSS (CLEVIOS P VP AI 4083 and CLEVIOS P VP CH 8000) were purchased from H. C. Starck GmbH. All chemicals and materials were purchased and used as received unless otherwise noted.

Device Fabrication. ITO-coated glass (from the China Southern Glass Holding Corp.) with a sheet resistance of 15−20 Ω per square was used as the substrate. The substrate was prepatterned by photolithography to give an effective device size of 15 mm^2. Prior to device fabrication, the substrates were thoroughly cleaned in sequential ultrasonic baths of acetone, isopropanol, detergent, deionized water, and isopropanol and dried in an oven. After 20 min of oxygen plasma cleaning, a 40-nm-thick PEDOT:PSS layer was spin-coated onto the ITO substrate followed by baking at 200 °C in nitrogen for 10 min. A 30-nm-thick PVK layer was subsequently spin-coated onto the top of the PEDOT:PSS layer from chlorobenzene solution. On top of the PVK, the emitting layer was spin-coated from G0:CN-DPASDB (blending ratio 100:0.15 by weight) *p*-xylene solution to form a 50-nm-thick film. After annealing the emission layer at 140 °C for 30 min, the electron injection layer was deposited. Three different types of EIL layers: pure $PFNR_2$, CsF doped $PFNR_2$, and pure CsF, were studied. The 20-nm-thick pure $PFNR_2$ film was spin-coated onto the EML from 0.1% methanol solution. For the hybrid EIL layer, the $PFNR_2$:CsF solutions were first prepared by blending the 1% $PFNR_2$ solution with the 0.1% CsF solution with weight ratios of 8:1, 4:1, and 2:1. Second, the blended solution was diluted with methanol to reach the $PFNR_2$ concentration at 0.1%. Finally, the blended solution was spin-coated onto the EML to form a 20-nm-thick film. To identify the optimal thickness of pure solution-processed CsF, various concentrations of the CsF solution were tested. After several rounds of tests, the 0.1% methanol solution gave the best device performance. Because the CsF film thickness is too thin to be measured by the surface profiler, we estimate the thickness to be approximately 1 nm based on the optimal thickness of the evaporated CsF film. For evaporated CsF, a 1-nm-thick CsF film was evaporated as the EIL. On top of the EIL, a 4-nm-thick Ba film followed by a 120-nm-thick Al film were evaporated using a shadow mask to form the top electrode at a base pressure of 1×10^{-4} Pa. The reported performance of each type of device is based on the mean values of eight devices. The device fabrication, except for the PEDOT:PSS coating, was conducted in a nitrogen atmosphere glovebox (Vacuum Atmosphere Co.) containing less than 10 ppm oxygen and moisture.

Device Characterization. The thickness of the organic films was determined using a Dektak 150 surface profiler. The current density

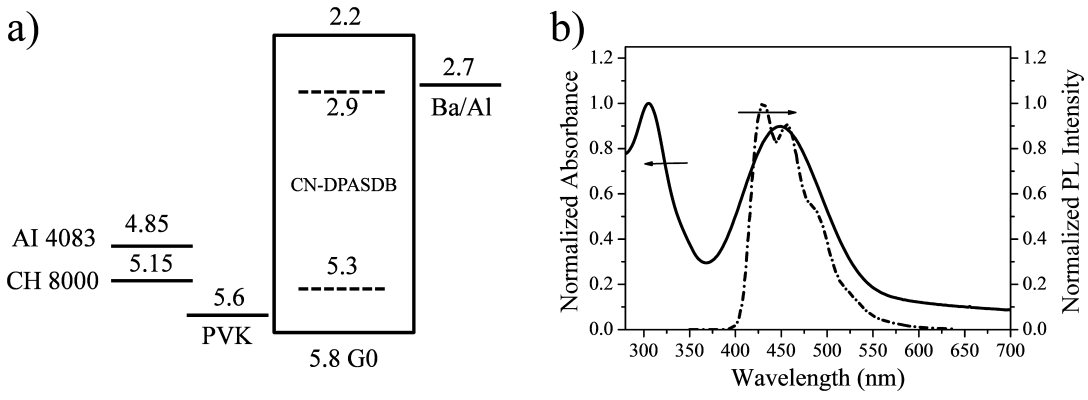

Figure 1. (a) Energy levels of the materials in each layer of the light-emitting device. (b) Normalized PL spectrum of the G0 solid film (dashed line) and the absorption spectrum of the CN-DPASDB solid film (solid line).

dx.doi.org/10.1021/am501207g | ACS Appl. Mater. Interfaces 2014, 6, 8345−8352

Table 1. Performance of WOLED Devices A, B, C, D, and E

						performance at 1000 cd m^{-2}			
device	V_{on} (V)	L_{max} (cd m^{-2})	LE$_{max}$ (cd A^{-1})	PE$_{max}$ (lm W^{-1})	EQE$_{max}$ (%)	V (V)	LE (cd A^{-1})	PE (lm W^{-1})	CIE[a] (x, y)
Device A	4.00	2.97 × 10^4	7.83 ± 0.14	4.75 ± 0.65	2.97 ± 0.05	5.75	7.40 ± 0.36	3.92 ± 0.27	(0.26, 0.28)
Device B	3.25	2.76 × 10^4	10.0 ± 0.25	9.46 ± 0.50	3.81 ± 0.09	6.00	6.57 ± 0.27	3.44 ± 0.14	(0.30, 0.33)
Device C	3.25	2.01 × 10^4	14.0 ± 0.33	11.0 ± 0.26	5.32 ± 0.12	6.00	9.51 ± 0.78	4.98 ± 0.55	(0.31, 0.36)
Device D	3.25	2.28 × 10^4	14.1 ± 0.69	12.1 ± 0.10	5.35 ± 0.26	5.75	8.10 ± 0.72	4.24 ± 0.38	(0.30, 0.33)
Device E	3.25	2.24 × 10^4	17.0 ± 0.30	15.6 ± 0.33	6.45 ± 0.11	6.25	9.41 ± 0.59	4.80 ± 0.32	(0.32, 0.37)

[a]Obtained at 13 mA cm^{-2}.

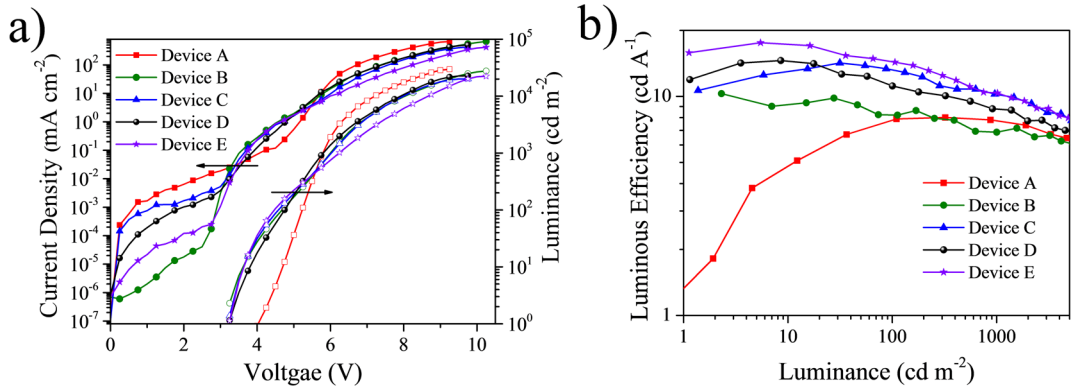

Figure 2. (a) J–V–L characteristics and (b) the dependence of the LE on the luminance of the devices. Device A: ITO/AI 4083/PVK/G0:CN-DPASDB/Ba/Al. Device B: ITO/CH 8000/PVK/G0:CN-DPASDB/Ba/Al. Device C: ITO/CH 8000/PVK/G0:CN-DPASDB/CsF (solution-processed)/Ba/Al. Device D: ITO/CH 8000/PVK/G0:CN-DPASDB/CsF (evaporated)/Ba/Al. Device E: ITO/CH 8000/PVK/G0:CN-DPASDB/PFNR$_2$:CsF/Ba/Al.

(J)–bias (V)–luminance (L) characteristics were measured using a Keithley 236 source meter and a silicon photodiode that was calibrated using a Konica Minolta Chroma Meter CS-200. The EL spectra and CIE coordinates were taken using a Photo Research PR-705 spectrometer. The AFM images were recorded using a Veeco DI MultiMode Nanoscope IIIa in tapping mode. The CPD was measured via scanning Kelvin probe microscopy (Kelvin Probe 5050 Technology) in N_2 atmosphere. Each data point in Figure 6b was the statistical mean of 20 measurements of each sample. The EQEs were measured using an integrating sphere (IS-080, Labsphere).

RESULTS

Figure 1a shows a schematic diagram of the device structure with the energy level of each layer. For the light-emitting layer, the highest occupied molecular orbital (HOMO) levels of G0 and CN-DPASDB are 5.8 and 5.3 eV, respectively, while the lowest unoccupied molecular orbital (LUMO) levels are 2.2 and 2.9 eV, respectively.[18,19] The HOMO of CN-DPASDB is 0.5 eV above the HOMO of G0, while the LUMO of CN-DPASDB is 0.7 eV below the LUMO of G0, implying that holes and electrons are readily trapped on the CN-DPASDB. As shown in Figure 1b, both the triphenyl axis and the backbone transitions are observed in the absorption spectrum of the CN-DPASDB solid film: the peak at approximately 306 nm is the absorption of the triphenyl axis, while the peak at approximately 449 nm is attributed to the π–π^* transitions in the backbone.[16] The excellent overlap between the photoluminescence (PL) spectrum of the G0 solid film and the backbone absorption of CN-DPASDB suggests efficient Förster energy transfer from the G0 host to the CN-DPASDB guest.[20,21]

To obtain the desired white color, a series of devices with different doping concentrations of CN-DPASDB in G0 were studied in the device configuration of ITO/AI 4083(40 nm)/PVK (30 nm)/G0:CN-DPASDB (50 nm)/Ba (4 nm)/Al (120 nm). With the doping concentration of 100:0.15 (G0:CN-DPASDB) by weight (Device A), the white electroluminescent (EL) spectrum exhibits balanced blue and yellow emissions, and the CIE coordinates of (0.26, 0.28) are close to the ideal equal-energy white point (0.33, 0.33). The optimized Device A shows a maximum luminance (L_{max}) of 2.97 × 10^4 cd m^{-2} at 9.25 V, a peak LE of 7.83 cd A^{-1}, and a maximum PE of 4.75 lm W^{-1} (Table 1). The highest EQE of 2.97% from Device A indicates that the balance of the holes and the electrons still has room to improve. Our early study shows that the G0 device is hole dominated.[19] Therefore, it is critical to suppress the holes while increasing the electrons to improve the device performance.

To suppress the holes, we replaced the high-conductivity PEDOT:PSS AI 4083 with low-conductivity PEDOT:PSS CH 8000 as the HIL layer in Device B. Compared with Device A, Device B shows a 27.8% improvement in LE$_{max}$ (from 7.83 cd A^{-1} to 10.0 cd A^{-1}), a 28.3% increase in EQE (from 2.97% to 3.81%), and a 99.2% improvement in PE$_{max}$ (from 4.75 lm W^{-1} to 9.46 lm W^{-1}) with a comparable maximum luminance (Table 1). To improve the electron injection, solution-processed CsF was implemented between the light-emitting layer and the Ba/Al cathode in Device C with the device configuration of ITO/CH 8000/PVK/G0:CN-DPASDB/CsF/Ba/Al. As a result, the LE$_{max}$ is further improved to 14.0 cd A^{-1}, the EQE increases to 5.32%, and the PE$_{max}$ reaches 11.0 lm W^{-1} (Table 1). However, due to the rough surface of the solution-processed CsF, the device performance with solution-processed CsF EIL is lower than with evaporated CsF EIL in Device D. To overcome this problem, we introduce a novel solution-processed EIL material by doping the conjugated polymer PFNR$_2$ with CsF. With the new EIL layer, Device E improves

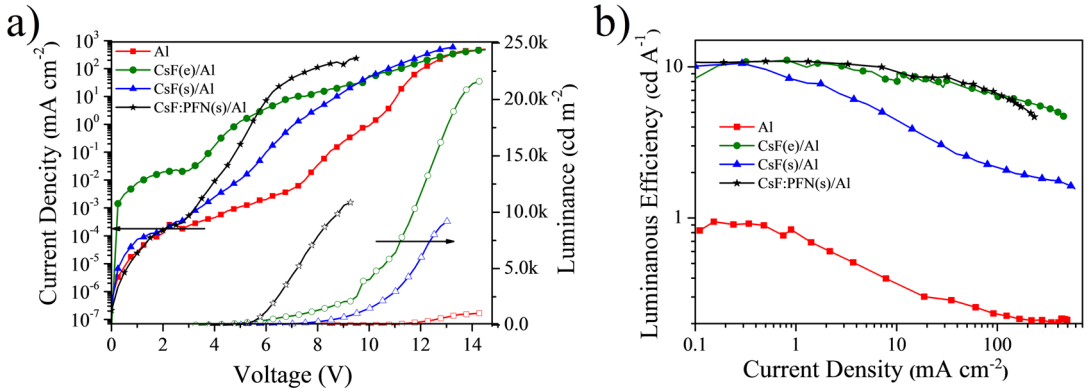

Figure 3. (a) $J-V-L$ characteristics and (b) the LE$-J$ characteristics of the devices with Al cathode and with different EIL. Red: no EIL. Green: evaporated CsF. Blue: solution-processed CsF. Black: $PFNR_2$ doped with CsF (4:1 by weight).

Table 2. Performances of WOLED Devices with Al Cathode and with Different EILs[a]

					performance at 1000 cd m^{-2}		
EIL/cathode	V_{on} (V)	L_{max} (cd m^{-2})	LE$_{max}$ (cd A^{-1})	PE$_{max}$ (lm W^{-1})	V (V)	LE (cd A^{-1})	PE (lm W^{-1})
no EIL/Al	8.50	0.11×10^4	0.88 ± 0.57	0.33 ± 0.19	14.3	0.23 ± 0.03	0.05 ± 0.01
CsF(e)/Al	3.50	2.16×10^4	9.81 ± 0.41	5.96 ± 0.45	7.50	8.31 ± 0.60	3.41 ± 0.32
CsF(s)/Al	5.25	0.92×10^4	9.55 ± 0.23	5.13 ± 0.50	9.75	2.52 ± 0.14	1.10 ± 0.15
CsF:$PFNR_2$/Al	4.00	1.09×10^4	11.8 ± 0.41	8.55 ± 0.74	6.25	7.97 ± 0.04	4.01 ± 0.02

[a]Note: e denotes evaporation process, and s denotes solution process.

LE$_{max}$ to 17.0 cd A^{-1}, EQE to 6.45%, and PE$_{max}$ to 15.6 lm W^{-1}, demonstrating one of the best fluorescent WOLED performances. All the device performances are detailed in Table 1. The $J-V-L$ characteristics and the luminous efficiency (LE) vs L of all the studied devices are illustrated in Figure 2.

DISCUSSION

Low- vs High-Conductivity Hole Injection Layer. High-conductivity PEDOT:PSS AI 4083 is the most widely used and successful HIL in solution-processed OLEDs.[22,23] Another type of PEDOT:PSS as HIL is the low-conductivity CH 8000. By simulating the $J-V$ characteristics, Cao and co-workers discovered that the hole concentration at the anode of the AI 4083 device was approximately 1 order of magnitude higher than that in the CH 8000 device.[7] It is suggested that the formation of a PSS-rich phase on the surface of CH 8000 enhances its electron blocking ability.[24] Because of the better electron blocking ability and the lower hole concentration, devices with CH 8000 HIL show much lower leakage current than devices with AI 4083 HIL, as shown in Figure 2a. Moreover, the work function of CH 8000 is 5.15 eV, higher than the work function of AI 4083, which is 4.85 eV.[25,26] The high work function of CH 8000 reduces the hole injection barrier between PEDOT and PVK, as shown in the device energy diagram (Figure 1a). As a result, the turn-on voltage V_{on} (defined as the voltage at 1 cd m^{-2}) of the device with CH 8000 HIL is 3.25 V, lower than the 4.0 V turn-on voltage of the device with AI 4083 HIL (Table 1 and Figure 2a).

CsF as Electron Injection Layer. Thermally evaporated CsF as an efficient EIL has been successfully demonstrated in OLEDs.[14,27] It is suggested that CsF adjusts the cathode's work function by doping the organic function layer with Cs ions,[28] and the deposition of aluminum can form AlF_3, thereby releasing metallic Cs and creating an ohmic contact for electron injection.[29] The fluoride-based EIL also protects the organic active layer from metal deposition and stabilizes the interface.[30] Solution-processed CsF has only been demonstrated as the electron extraction layer in organic photovoltaic devices.[31,32] To study solution-processed CsF as an EIL in OLEDs, we fabricated OLED devices without any EIL, with thermally evaporated CsF EIL, and with solution-processed CsF EIL in the device configuration of ITO/CH 8000/PVK/G0:CN-DPASDB/EIL/Al. The $J-V-L$ and LE$-J$ characteristics of the device are illustrated in Figure 3. The device performance is summarized in Table 2.

As shown in Figure 3, the device with no EIL lacks efficient electron injection, resulting in a very low efficiency (LE$_{max}$ = 0.88 cd A^{-1}). With thermally evaporated CsF EIL, the device performance is substantially improved. LE$_{max}$ reaches 9.81 cd A^{-1}, and the maximum luminance reaches 2.16×10^4 cd m^{-2}. In addition, due to the efficient electron injection, the turn-on voltage V_{on} is lowered from 8.50 V in the device with no EIL to only 3.50 V (Table 2). In comparison, though the device with solution-processed CsF EIL has a similar maximum LE of 9.55 cd A^{-1}, the maximum luminance is only 0.92×10^4 cd m^{-2}, and the turn-on voltage is as high as 5.25 V. Moreover, the device LE exhibits a greater roll-off at high current density, as shown in Figure 3b. We suspect that the apparent performance difference is due to the surface morphology of the CsF solid film achieved by different processes.

Figure 4a–c, respectively, shows the atomic force microscopy (AFM) images of the emission layer (G0:CN-DPASDB), the evaporated CsF on the emission layer, and the spin-coated CsF on the emission layer. The images clearly show that the evaporated CsF forms a smooth, uniform, and pinhole-free film on top of the EML with a RMS surface roughness of approximately 0.3 nm. In contrast, the spin-coated CsF film exhibits many spikes with a RMS surface roughness of approximately 0.7 nm. Because CsF is highly polar, once spin-coated onto a hydrophobic organic layer, CsF will aggregate and create spikes. Similar phenomena have been observed in solution-processed conjugated polyelectrolytes and

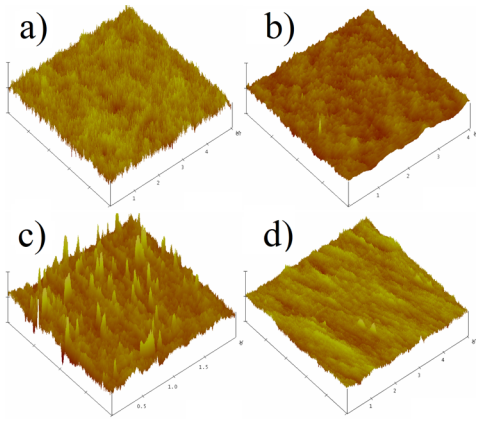

Figure 4. AFM images of (a) the EML surface deposited atop ITO/PEDOT:PSS/PVK, (b) the evaporated CsF surface deposited atop the emission layer, (c) the spin-coated CsF surface deposited atop the emission layer, and (d) the $PFNR_2$:CsF = 4:1 surface spin-coated atop the emission layer. RMS is 0.5, 0.3, 0.7, and 0.3 nm, respectively.

solution-processed inorganic salts on an organic layer.[33−35] However, the smooth evaporated CsF film creates a larger leakage current than the spiky solution-processed CsF film, as shown in Figure 3a. We suspect that some evaporated CsF may migrate into the underlying layer, thereby causing the increased leakage current.[36] Nevertheless, the leakage current density is less than 2×10^{-2} mA cm^{-2}, which is still on the same order of magnitude as that of the OLED devices with evaporated CsF EIL published in other papers.[12,14]

Novel Hybrid Electron Injection Layer. To obtain a smooth CsF film during solution processing, we introduce a hybrid EIL by doping CsF into the water/alcohol-soluble conjugated polymer electron injection material $PFNR_2$. To investigate the effects of the hybrid EIL on device performance, white OLEDs with the structure of ITO/CH 8000 (40 nm)/PVK (30 nm)/G0:CN-DPASDB (100:0.15 wt %) (50 nm)/EIL/Ba (4 nm)/Al (120 nm) were fabricated by varying the doping concentration of CsF in the host $PFNR_2$ by weight. The *J*−*V*−*L* and LE−*L* characteristics of the devices are shown in Figure 5, and the detailed data are listed in Table 3.

The solution-processed pure CsF EIL performs better with a Ba/Al cathode than it does with an Al cathode. With the additional Ba, the device more than doubles the maximum luminance (from 0.92×10^4 to 2.01×10^4 cd m^{-2}) and increases the luminous efficiency by 49% (Tables 2 and 3) because the deposition of the low work function and high reactivity of Ba on CsF liberates more Cs ions, similar to the effect of a LiF/Ca/Al cathode.[37] For the same reason, an additional layer of Ba on spin-coated CsF improves the device performance to near the level of the evaporated CsF EIL device, as shown in Figure 2 and Table 1. However, the leakage current is still high (Figure 5a).

The water/alcohol-soluble conjugated polymer $PFNR_2$ has been widely used as the EIL in OLEDs for its unique interface modification ability, processability in environmental friendly solvents, and multilayer device engineering without interface mixing.[14,38−40] However, with pure $PFNR_2$ (CsF doping concentration equals zero) as the EIL, the device underperforms at high current density. The maximum brightness only reaches 1.16×10^4 cd m^{-2}. With slight CsF doping ($PFNR_2$:CsF = 8:1), the performance at high current density recovers. Not only does the maximum brightness increase to 1.51×10^4 cd m^{-2}, but the maximum EQE also increases from 5.20% to 5.73%. The best device performance is achieved with a CsF doping concentration of $PFNR_2$:CsF = 4:1. The device exhibits a maximum LE of 17.0 cd A^{-1} and a maximum PE of 15.6 lm W^{-1} with a maximal brightness of 2.24×10^4 cd m^{-2}. At the brightness of 1000 cd m^{-2}, the LE drops to 9.41 cd A^{-1}, and the PE becomes 4.80 lm W^{-1}. The CRI of the device is 64. Upon increasing the doping concentration of CsF, the device performance begins to drop (Table 3). As shown in Figure 5a, the devices with the hybrid EIL have a much lower leakage current than the device with pure CsF EIL. As illustrated in Figure 4d, the hybrid EIL forms a smooth film on top of the EML with a RMS surface roughness of ca. 0.3 nm and without any spikes.

To study the mechanism of the hybrid electron injection layer, electron-dominated devices ITO/Al (60 nm)/G0:CN-DPASDB (100:0.15 wt % 50 nm)/EIL/Ba (4 nm)/Al (120 nm) were fabricated. The *J*−*V* characteristic curves are depicted in Figure 6a. With no EIL, the device's electron current is low. With pure $PFNR_2$ ($PFNR_2$:CsF = 1:0) as the EIL, the electron current increases while below 9 V. Above 9 V, the electron injection of the device becomes less efficient, leading to a decreased electron current. With pure CsF ($PFNR_2$:CsF = 0:1) as the EIL, the electron current of the device is the highest among all of the devices. In between, however, the devices' electron currents do not exhibit a clear trend following the CsF doping concentration.

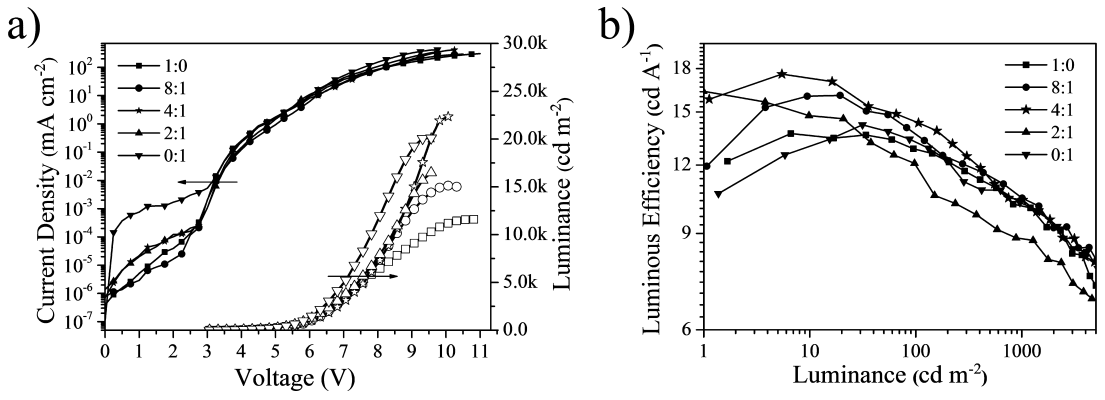

Figure 5. (a) *J*−*V*−*L* characteristics and (b) the LE−*L* characteristics of the WOLED devices with solution-processed EIL using different ratios of $PFNR_2$ to CsF by weight.

dx.doi.org/10.1021/am501207g | ACS Appl. Mater. Interfaces 2014, 6, 8345−8352

Table 3. Performance of OLEDs with Different EILs

						performance at 1000 cd m^{-2}				
$PFNR_2$:CsF	V_{on} (V)	L_{max} (cd m^{-2})	LE_{max} (cd A^{-1})	PE_{max} (lm W^{-1})	EQE_{max} (%)	V (V)	LE (cd A^{-1})	PE (lm W^{-1})	CIE[a] (x, y)	CRI[a]
1:0	3.25	1.16×10^4	13.7 ± 0.20	12.3 ± 0.81	5.20 ± 0.03	6.00	9.12 ± 0.12	4.65 ± 0.14	(0.33 ,0.39)	61
8:1	3.25	1.51×10^4	15.8 ± 0.37	12.6 ± 0.57	5.73 ± 0.52	6.25	9.57 ± 0.31	4.76 ± 0.54	(0.32, 0.38)	63
4:1	3.25	2.24×10^4	17.0 ± 0.30	15.6 ± 0.33	6.45 ± 0.11	6.25	9.41 ± 0.59	4.80 ± 0.32	(0.32, 0.37)	64
2:1	3.25	1.65×10^4	15.1 ± 0.83	13.3 ± 0.98	5.74 ± 0.31	6.00	8.23 ± 0.70	4.14 ± 0.35	(0.31, 0.35)	68
0:1	3.25	2.01×10^4	14.2 ± 0.63	11.9 ± 0.61	5.38 ± 0.24	6.00	9.37 ± 0.78	4.85 ± 0.45	(0.31, 0.36)	65

[a]Obtained at 13 mA cm^{-2}.

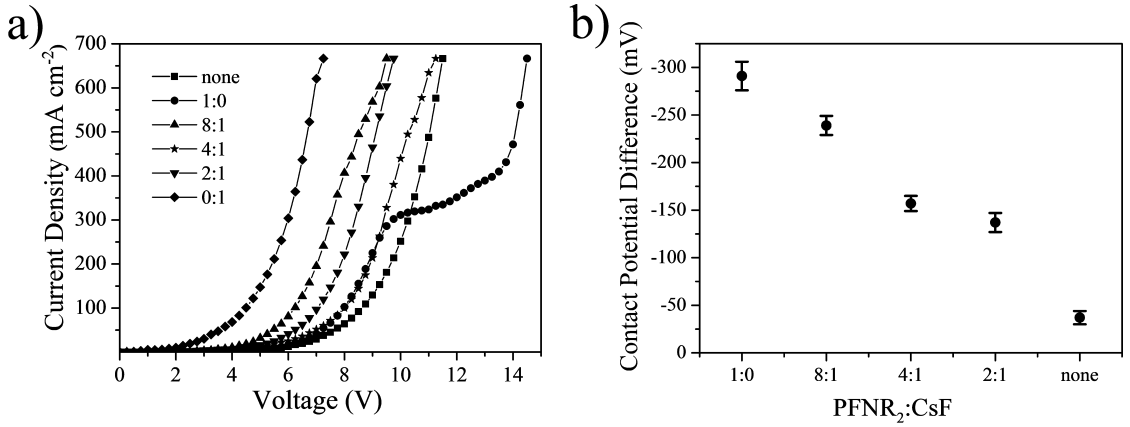

Figure 6. (a) J–V characteristics of the electron dominated devices and (b) the contact potential difference (CPD) of EIL at different ratios of $PFNR_2$ to CsF (1:0, 8:1, 4:1, 2:1, 0:1) and with no EIL (none).

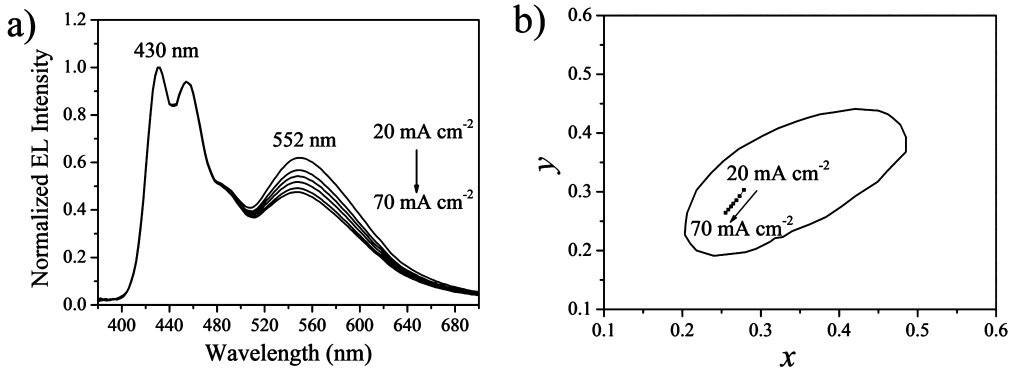

Figure 7. (a) EL spectra and (b) CIE of the device [ITO/PEDOT:PSS (40 nm)/PVK (30 nm)/EML (50 nm)/$PFNR_2$:CsF (= 4:1)/Ba (4 nm)/Al (120 nm)] under different current densities (20 to 70 mA cm^{-2}). The circle in (b) represents the white color region. Any color that falls inside the circle is considered as white color.

To fully understand the hybrid EIL's working mechanism, we must understand the $PFNR_2$ and CsF's working mechanisms. As discussed in many publications,[14,41,42] $PFNR_2$ forms a dipole layer that elevates the vacuum level at the cathode side, thereby reducing the electron injection barrier. For CsF, as discussed earlier, the dissociation of CsF causes Cs doping at the polymer interface, resulting in a lower electron injection barrier. Moreover, the deposition of aluminum can form AlF_3, releasing metallic Cs, which creates an ohmic contact for electron injection. When CsF is doped into $PFNR_2$ they work together to facilitate the electron injection. However, they weaken each other's effect because the dissociated Cs^+ ions are attracted to the negatively charged amino group of the $PFNR_2$, reducing the strength of the interfacial dipole created by $PFNR_2$. Surface potential measurement by scanning Kelvin probe microscopy (SKPM) was employed to examine the weakening of the interfacial dipole by the addition of CsF. With no EIL, the contact potential difference (CPD) between the probe tip and the emission layer surface was approximately −53 mV. After spin-coating with pure $PFNR_2$, the CPD became −290 mV, reducing the surface potential by 0.24 V, indicating that a strong dipole layer is formed.[39,43−46] As the CsF doping concentration increases ($PFNR_2$:CsF = 8:1, 4:1, 2:1), the CPD monotonically decreases, showing that the interfacial dipole strength is weakened by the CsF (Figure 6b).

With a low concentration of CsF doping ($PFNR_2$:CsF = 8:1), the electron current significantly increases (Figure 6a). This result suggests that the additional small amount of CsF works favorably to improve the electron injection. Though the interfacial dipole strength drops, the ohmic contact between the cathode and the EIL formed by the metallic Cs helps overcome the vacuum level drop. Upon doubling the CsF doping concentration to $PFNR_2$:CsF = 4:1, the electron current substantially decreases (Figure 6a). The creation of the ohmic

contact by the metallic Cs cannot compensate for the lowering of the interfacial dipole by the Cs^+ ion. At this specific concentration, an overall charge balance of holes and electrons is reached, and the light-emitting device exhibits the best performance (Figure 5, Table 3). Upon further increasing the CsF concentration to $PFNR_2$:CsF = 2:1, Cs-doping into the polymer becomes the dominant effect and reduces the electron injection barrier, increasing the electron current. However, excessive electrons adversely affect the performance of light-emitting devices, as demonstrated in Figure 5 and Table 3.

Color Stability. The EL spectra of the device with the best performance under difference current densities are shown in Figure 7a. Two emission peaks at approximately 430 and 552 nm are clearly observed, which can be attributed to the emission from the host G0 and the guest CN-DPASDB, respectively. Although white is achieved by a two color emission system, the saturated blue emission from G0 and the broad-band yellow emission from CN-DPASDB cause the white emission to cover most of the visible spectrum. As the current density increases, the relative emission intensity from CN-DPASDB decreases. Because the voltage required to excite the yellow emission of CN-DPASDB is lower than the voltage to excite the blue emission of G0, it is expected that the emission color will shift toward blue with increasing voltage.[47] As the relative blue emission intensity increases, the CIE coordinates also move toward the blue region, as shown in Figure 7b. Nonetheless, the color coordinates are still within the white color region. At 13 mA cm^{-2}, the color coordinates are (0.32, 0.37) with a color rendering index of 64, which is suitable for solid-state lighting.

CONCLUSIONS

In conclusion, by doping a deep blue fluorescent conjugated dendrimer G0 with a fluorescent broad-band yellow emitter CN-DPASDB, a highly efficient electrofluorescent WOLED is achieved by solution process. Using a low-conductivity anode buffer layer and CsF-doped $PFNR_2$ as a novel EIL, the device exhibits one of the best reported fluorescent WOLED performances with 17.0 cd A^{-1} luminous efficiency, 15.6 lm W^{-1} power efficiency, and 2.24×10^4 cd m^{-2} luminance. The solution-processed hybrid EIL (CsF doped $PFNR_2$) works together with the low-conductivity HIL (PEDOT:PSS CH 8000) to achieve balanced carriers for state-of-the-art device performance. The solution process for all of the functional layers demonstrates a huge potential for large-area, low-cost WOLED lighting panel manufacturing.

AUTHOR INFORMATION

Corresponding Author

*E-mail: jianwang@scut.edu.cn (J.W.)

Author Contributions

The manuscript was written through contributions of all authors. All authors have given approval to the final version of the manuscript.

Notes

The authors declare no competing financial interest.

ACKNOWLEDGMENTS

We are deeply grateful to the Ministry of Science and Technology (973 Program 2009CB623604, 2009CB930604, 2013CB834705) and National Nature Science Foundation of China (61076116, 51373057) for their financial support.

REFERENCES

(1) Tang, C. W.; VanSlyke, S. A. Organic Electroluminescent Diodes. *Appl. Phys. Lett.* **1987**, *51*, 913−915.
(2) Burroughes, J. H.; Bradley, D. D. C.; Brown, A. R.; Marks, R. N.; Mackay, K.; Friend, R. H.; Born, P. L.; Holmes, A. B. Light Emitting Diodes Based on Conjugated Polymers. *Nature* **1990**, *347*, 539−541.
(3) Kido, J.; Kimura, M.; Nagai, K. Multilayer White Light-emitting Organic Electroluminescent Device. *Science* **1995**, *267*, 1332−1334.
(4) D'Andrade, B. W.; Forrest, S. R. White Organic Light-emitting Devices for Solid-state Lighting. *Adv. Mater.* **2004**, *16*, 1585−1595.
(5) Misra, A.; Kumar, P.; Kamalasanan, M. N.; Chandra, S. White Organic LEDs and Their Recent Advancements. *Semicond. Sci. Technol.* **2006**, *21*, R35−R47.
(6) Sasabe, H.; Takamatsu, J.; Motoyama, T.; Watanabe, S.; Wagenblast, G.; Langer, N.; Molt, O.; Fuchs, E.; Lennartz, C.; Kido, J. High-efficiency Blue and White Organic Light-emitting Devices Incorporating a Blue Iridium Carbene Complex. *Adv. Mater.* **2010**, *22*, 5003−5007.
(7) Zou, J.; Wu, H.; Lam, C. S.; Wang, C.; Zhu, J.; Zhong, C.; Hu, S.; Ho, C. L.; Zhou, G. J.; Wu, H.; Choy, W. C.; Peng, J.; Cao, Y.; Wong, W. Y. Simultaneous Optimization of Charge-carrier Balance and Luminous Efficacy in Highly Efficient White Polymer Light-emitting Devices. *Adv. Mater.* **2011**, *23*, 2976−2980.
(8) Baldo, M. A.; O'Brien, D. F.; You, Y.; Shoustikov, A.; Sibley, S.; Thompson, M. E.; Forrest, S. R. Highly Efficient Phosphorescent Eemission from Organic Electroluminescent Devices. *Nature* **1998**, *395*, 151−154.
(9) He, G.; Pfeiffer, M.; Leo, K.; Hofmann, M.; Birnstock, J.; Pudzich, R.; Salbeck, J. High-efficiency and Low-voltage p-i-n Electrophosphorescent Organic Light-emitting Diodes with Double-emission Layers. *Appl. Phys. Lett.* **2004**, *85*, 3911−3913.
(10) Baldo, M. A.; Lamansky, S.; Burrows, P. E.; Thompson, M. E.; Forrest, S. R. Very High-efficiency Green Organic Light-emitting Devices Based on Electrophosphorescence. *Appl. Phys. Lett.* **1999**, *75*, 4−6.
(11) Zhang, Z.; Wang, Q.; Dai, Y.; Liu, Y.; Wang, L.; Ma, D. High Efficiency Fluorescent White Organic Light-emitting Diodes with Red, Green and Blue Separately Monochromatic Emission Layers. *Org. Electron.* **2009**, *10*, 491−495.
(12) Yu, L.; Liu, J.; Hu, S.; He, R.; Yang, W.; Wu, H.; Peng, J.; Xia, R.; Bradley, D. D. C. Red, Green, and Blue Light-emitting Polyfluorenes Containing a Dibenzothiophene-S,S-Dioxide Unit and Efficient High-color-rendering-index White-light-emitting Diodes Made Therefrom. *Adv. Funct. Mater.* **2013**, *23*, 4366−4376.
(13) Huang, J.; Hou, W. J.; Li, J. H.; Li, G.; Yang, Y. Improving the Power Efficiency of White Light-emitting Diode by Doping Electron Transport Material. *Appl. Phys. Lett.* **2006**, *89*, 133509−1−133509−3.
(14) Xue, S.; Yao, L.; Shen, F.; Gu, C.; Wu, H.; Ma, Y. Highly Efficient and Fully Solution-processed White Electroluminescence Based on Fluorescent Small Molecules and a Polar Conjugated Polymer as the Electron-injection Material. *Adv. Funct. Mater.* **2012**, *22*, 1092−1097.
(15) Jiang, Y.; Wang, J. Y.; Ma, Y.; Cui, Y. X.; Zhou, Q. F.; Pei, J. Large Rigid Blue-emitting Pi-conjugated Stilbenoid-based Dendrimers: Synthesis and Properties. *Org. Lett.* **2006**, *8*, 4287−4290.
(16) Li, Y. P.; Shen, F. Z.; Wang, H.; He, F.; Xie, Z. Q.; Zhang, H. Y.; Wang, Z. M.; Liu, L. L.; Li, F.; Hanif, M.; Ye, L.; Ma, Y. G. Supramolecular Network Conducting the Formation of Uniaxially Oriented Molecular Crystal of Cyano Substituted Oligo(p-phenylene vinylene) and Its Amplified Spontaneous Emission (ASE) Behavior. *Chem. Mater.* **2008**, *20*, 7312−7318.
(17) Huang, F.; Wu, H. B.; Wang, D.; Yang, W.; Cao, Y. Novel Electroluminescent Conjugated Polyelectrolytes Based on Polyfluorene. *Chem. Mater.* **2004**, *16*, 708−716.
(18) Liu, S.; Li, F.; Diao, Q.; Ma, Y. Aggregation-induced Enhanced Emission Materials for Efficient White Organic Light-emitting Devices. *Org. Electron.* **2010**, *11*, 613−617.
(19) Wang, L.; Jiang, Y.; Luo, J.; Zhou, Y.; Zhou, J.; Wang, J.; Pei, J.; Cao, Y. Highly Efficient and Color-stable Deep-blue Organic Light-

emitting Diodes Based on a Solution-processible Dendrimer. *Adv. Mater.* **2009**, *21*, 4854−4858.
(20) Gong, X.; Ostrowski, J. C.; Moses, D.; Bazan, G. C.; Heeger, A. J. Electrophosphorescence from a Polymer Guest-Host System with an Iridium Complex as Guest: Forster Energy Transfer and Charge Trapping. *Adv. Funct. Mater.* **2003**, *13*, 439−444.
(21) Zou, J. H.; Liu, J.; Wu, H. B.; Yang, W.; Peng, J. B.; Cao, Y. High-efficiency and Good Color Quality White Light-emitting Devices Based on Polymer Blend. *Org. Electron.* **2009**, *10*, 843−848.
(22) Kim, J. S.; Granström, M.; Friend, R. H.; Johansson, N.; Salaneck, W. R.; Daik, R.; Feast, W. J.; Cacialli, F. Indium-tin Oxide Treatments for Single- and Double-layer Polymeric Light-emitting Diodes: the Relation between the Anode Physical, Chemical, and Morphological Properties and the Device Performance. *J. Appl. Phys.* **1998**, *84*, 6859−6870.
(23) Elschner, A.; Bruder, F.; Heuer, H. W.; Jonas, F.; Karbach, A.; Kirchmeyer, S.; Thurm, S. PEDT/PSS for Efficient Hole-injection in Hybrid Organic Light-emitting Diodes. *Synth. Met.* **2000**, *111*, 139−143.
(24) Koch, N.; Elschner, A.; Johnson, R. L. Green Polyfluorene-conducting Polymer Interfaces: Energy Level Alignment and Device Performance. *J. Appl. Phys.* **2006**, *100*, 024512-1−024512-5.
(25) Wu, S.; Han, S.; Zheng, Y.; Zheng, H.; Liu, N.; Wang, L.; Cao, Y.; Wang, J. pH-neutral PEDOT:PSS as Hole Injection Layer in Polymer Light Emitting Diodes. *Org. Electron.* **2011**, *12*, 504−508.
(26) Koch, N.; Elschner, A.; Rabe, J. P.; Johnson, R. L. Work Function Independent Hole-injection Barriers Between Pentacene and Conducting Polymers. *Adv. Mater.* **2005**, *17*, 330−335.
(27) Li, Y.; Wu, H.; Lam, C. S.; Chen, Z.; Wu, H.; Wong, W. Y.; Cao, Y. Highly Efficient Blue and All-phosphorescent White Polymer Light-emitting Devices Based on Polyfluorene Host. *Org. Electron.* **2013**, *14*, 1909−1915.
(28) Greczynski, G.; Fahlman, M.; Salaneck, W. R. Hybrid Interfaces of Poly(9,9-dioctylfluorene) Employing Thin Insulating Layers of CsF: a Photoelectron Spectroscopy Study. *J. Chem. Phys.* **2001**, 8628−8636.
(29) Piromreun, P.; Oh, H.; Shen, Y.; Malliaras, G. G.; Scott, J. C.; Brock, P. J. Role of CsF on Electron Injection into a Conjugated Polymer. *Appl. Phys. Lett.* **2000**, *77*, 2403−2045.
(30) Le, Q. T.; Yan, L.; Gao, Y.; Mason, M. G.; Giesen, D. J.; Tang, C. W. Photoemission Study of Aluminum/Tris-(8-hydroxyquinoline) Aluminum and Aluminum/LiF/Tris-(8-hydroxyquinoline) Aluminum Interfaces. *J. Appl. Phys.* **2000**, *87*, 375−379.
(31) Reinhard, M.; Hanisch, J.; Zhang, Z.; Ahlswede, E.; Colsmann, A.; Lemmer, U. Inverted Organic Solar Cells Comprising a Solution-Processed Cesium Fluoride Interlayer. *Appl. Phys. Lett.* **2011**, *98*, 053303-1−053303-3.
(32) Huang, J.; Li, G.; Yang, Y. A Semi-transparent Plastic Solar Cell Fabricated by a Lamination Process. *Adv. Mater.* **2008**, *20*, 415−419.
(33) Georgiadou, D. G.; Vasilopoulou, M.; Palilis, L. C.; Petsalakis, I. D.; Theodorakopoulos, G.; Constantoudis, V.; Kennou, S.; Karantonis, A.; Dimotikali, D.; Argitis, P. All-Organic Sulfonium Salts Acting as Efficient Solution Processed Electron Injection Layer for PLEDs. *ACS Appl. Mater. Interfaces* **2013**, *5*, 12346−12354.
(34) Garcia, A.; Bakus Ii, R. C.; Zalar, P.; Hoven, C. V.; Brzezinski, J. Z.; Nguyen, T. Q. Controlling Ion Motion in Polymer Light-Emitting Diodes Containing Conjugated Polyelectrolyte Electron Injection Layers. *J. Am. Chem. Soc.* **2011**, *133*, 2492−2498.
(35) Hsiao, C. C.; Hsiao, A. E.; Chen, S. A. Design of Hole Blocking Layer with Electron Transport Channels for High Performance Polymer Light-Emitting Diodes. *Adv. Mater.* **2008**, *20*, 1982−1988.
(36) Niu, Y. H.; Ma, H.; Xu, Q.; Jen, A. K. Y. High-efficiency Light-emitting Diodes Using Neutral Surfactants and Aluminum Cathode. *Appl. Phys. Lett.* **2005**, *86*, 083504−1−083504−3.
(37) Brown, T. M.; Friend, R. H.; Millard, I. S.; Lacey, D. J.; Burroughes, J. H.; Cacialli, F. Efficient Electron Injection in Blue-emitting Polymer Light-emitting Diodes with LiF/Ca/Al Cathodes. *Appl. Phys. Lett.* **2001**, *79*, 174−176.
(38) Wu, H. B.; Huang, F.; Mo, Y. Q.; Yang, W.; Wang, D. L.; Peng, J. B.; Cao, Y. Efficient Electron Injection from a Bilayer Cathode Consisting of Aluminum and Alcohol-/Water-soluble Conjugated Polymers. *Adv. Mater.* **2004**, *16*, 1826−1830.
(39) Lv, M.; Li, S.; Jasieniak, J. J.; Hou, J.; Zhu, J.; Tan, Z.; Watkins, S. E.; Li, Y.; Chen, X. A Hyperbranched Conjugated Polymer as the Cathode Interlayer for High Performance Polymer Solar Cells. *Adv. Mater.* **2013**, *25*, 6889−6894.
(40) Zheng, H.; Zheng, Y.; Liu, N.; Ai, N.; Wang, Q.; Wu, S.; Zhou, J.; Hu, D.; Yu, S.; Han, S.; Xu, W.; Luo, C.; Meng, Y.; Jiang, Z.; Chen, Y.; Li, D.; Huang, F.; Wang, J.; Peng, J.; Cao, Y. All-solution Processed Polymer Light-emitting Diode Displays. *Nat. Commun.* **2013**, *4*, 1971−1−1971−7.
(41) Wu, H.; Huang, F.; Peng, J.; Cao, Y. High-efficiency Electron Injection Cathode of Au for Polymer Light-emitting Devices. *Org. Electron.* **2005**, *6*, 118−128.
(42) Wang, L.; Liang, B.; Huang, F.; Peng, J.; Cao, Y. Utilization of Water/Alcohol-soluble Polyelectrolyte as an Electron Injection Layer for Fabrication of High-efficiency Multilayer Saturated Red-phosphorescence Polymer Light-emitting Diodes by Solution Processing. *Appl. Phys. Lett.* **2006**, *89*, 15115-1−151115-3.
(43) Wang, Q.; Zhou, Y.; Zheng, H.; Shi, J.; Li, C.; Su, C. Q.; Wang, L.; Luo, C.; Hu, D.; Pei, J.; Wang, J.; Peng, J.; Cao, Y. Modifying Organic/Metal Interface via Solvent Treatment to Improve Electron Injection in Organic Light Emitting Diodes. *Org. Electron.* **2011**, *12*, 1858−1863.
(44) Wang, Q.; Chen, Y.; Zheng, Y.; Ai, N.; Han, S.; Xu, W.; Jiang, Z.; Meng, Y.; Hu, D.; Peng, J.; Wang, J.; Cao, Y. Solvent Treatment as an Efficient Anode Modification Method to Improve Device Performance of Polymer Light-emitting Diodes. *Org. Electron.* **2013**, *14*, 548−553.
(45) He, Z.; Zhong, C.; Huang, X.; Wong, W. Y.; Wu, H.; Chen, L.; Su, S.; Cao, Y. Simultaneous Enhancement of Open-circuit Voltage, Short-circuit Current Density, and Fill Factor in Polymer Solar Cells. *Adv. Mater.* **2011**, *23*, 4636−4643.
(46) Zhou, H.; Zhang, Y.; Seifter, J.; Collins, S.; Luo, C.; Bazan, G.; Nguyen, T. Q.; Heeger, A. High-efficiency Polymer Solar Cells Enhanced by Solvent Treatment. *Adv. Mater.* **2013**, *25*, 1646−1652.
(47) D'Andrade, B. W.; Holmes, R. J.; Forrest, S. R. Efficient Organic Electrophosphorescent White-light-emitting Device with a Triple Doped Emissive Layer. *Adv. Mater.* **2004**, *16*, 624−628.